

# Sequential Projected Newton method for regularization of nonlinear least squares problems

J Cornelis & W Vanroose

Department of Mathematics, University of Antwerp, 2020 Antwerp, Belgium

E-mail: jeffrey.cornelis@uantwerp.be

12 May 2021

**Abstract.** We develop an efficient algorithm for the regularization of nonlinear inverse problems based on the discrepancy principle. We formulate the problem as an equality constrained optimization problem, where the constraint is given by a least squares data fidelity term and expresses the discrepancy principle. The objective function is a convex regularization function that incorporates some prior knowledge, such as the total variation regularization function. Using the Jacobian matrix of the nonlinear forward model, we consider a sequence of quadratically constrained optimization problems that can all be solved using the Projected Newton method. We show that the solution of the sub-problem results in a descent direction for an exact merit function. This merit function can then be used to describe a formal line-search method. We also formulate a slightly more heuristic approach that simplifies the algorithm and results in a significant computational improvement. We illustrate the robustness and effectiveness of our approach using a number of numerical experiments. We consider Talbot-Lau x-ray phase contrast imaging as application.

*Keywords:* Projected Newton method, inverse problem, regularization, constrained optimization, Talbot-Lau phase contrast imaging

## 1. Introduction

In this manuscript we consider the regularized nonlinear least squares problem

$$\min_{x \in \mathbb{R}^n} \Psi(x) \quad \text{subject to} \quad \frac{1}{2} \|s(x) - b\|^2 \leq \frac{\sigma^2}{2} \quad (1)$$

where  $\Psi : \mathbb{R}^n \rightarrow \mathbb{R}$  is a convex twice continuously differentiable function. The function  $s : \mathbb{R}^n \rightarrow \mathbb{R}^m$  with  $m \geq n$  models some nonlinear forward operation and  $b \in \mathbb{R}^m$  is some data contaminated with measurement errors or noise. Here,  $\sigma$  is an estimate of the noise-level, i.e.  $\sigma \approx \|b_{ex} - b\|$ , for some “exact” data  $b_{ex}$ . In the following we assume that the unconstrained solution of the least squares problem is below the noise-level, i.e. that  $\min_x \|s(x) - b\| \leq \sigma$ . This implies that the constraint in (1) is feasible and thus there exists at least one local solution.

Furthermore, we assume  $s(x)$  has component functions  $s_i(x) : \mathbb{R}^n \rightarrow \mathbb{R}$  for  $i = 1, \dots, m$  that are all continuously differentiable, such that the Jacobian matrix

$$J(x) = \left( \frac{\partial s_i(x)}{\partial x_j} \right)_{i,j} = \begin{pmatrix} \frac{\partial s_1(x)}{\partial x_1} & \cdots & \frac{\partial s_1(x)}{\partial x_n} \\ \vdots & \ddots & \vdots \\ \frac{\partial s_m(x)}{\partial x_1} & \cdots & \frac{\partial s_m(x)}{\partial x_n} \end{pmatrix} \in \mathbb{R}^{m \times n}$$

is well-defined. Let us denote the constraint function as  $c(x) = \frac{1}{2} \|s(x) - b\|^2 - \frac{\sigma^2}{2}$ . It is an easy calculation to verify that the gradient of the constraint function is given by  $\nabla c(x) = J(x)^T (s(x) - b)$ .

In most cases of interest we can show that the inequality constraint in (1) becomes active for the solution  $x^*$  and can thus be replaced by an equality constraint.

**Lemma 1.1.** *Suppose  $x^*$  is a local solution of (1) with  $\nabla \Psi(x^*) \neq 0$  and  $\nabla c(x^*) \neq 0$ . Then  $\|s(x^*) - b\| = \sigma$  and there exists a unique Lagrange multiplier  $\lambda^* > 0$  such that*

$$\begin{cases} \nabla \Psi(x^*) + \lambda^* \nabla c(x^*) = 0, \\ c(x^*) = 0. \end{cases} \quad (2)$$

*Proof.* The linear independence constraint qualification (LICQ) trivially holds for  $x^*$  since we only have one constraint and we assume that  $\nabla c(x^*) \neq 0$ . Hence, there exists a Lagrange multiplier  $\lambda^* \in \mathbb{R}$  such that the Karuhn-Kush-Tucker or KKT conditions are satisfied [1]:

$$\begin{cases} \nabla \Psi(x^*) + \lambda^* \nabla c(x^*) = 0, \\ \lambda^* c(x^*) = 0 \\ c(x^*) \leq 0, \quad \lambda^* \geq 0. \end{cases}$$

Suppose that  $\|s(x^*) - b\| \neq \sigma$ , i.e.  $c(x^*) \neq 0$ , then it follows from the complementarity condition that  $\lambda^* = 0$ . This in turn means that  $\nabla \Psi(x^*) = 0$  which contradicts our assumption that  $\nabla \Psi(x^*) \neq 0$ . Hence, it follows that  $\lambda^* > 0$  and  $\|s(x^*) - b\| = \sigma$  and that  $(x^*, \lambda^*)$  satisfies (2). Uniqueness of the Lagrange multiplier easily follows from the fact  $\nabla c(x^*) \neq 0$ .  $\square$

The conditions in lemma 1.1 are very mild since  $\nabla \Psi(x^*) = 0$  means that  $x^*$  is an unconstrained minimizer of the convex regularization function. Similarly we have that  $\nabla c(x^*) = 0$  expresses the first order necessary optimality condition of the unconstrained optimization problem  $\operatorname{argmin} \|s(x) - b\|$ .

Note that (2) are precisely the KKT conditions of the equality constrained problem

$$\min_{x \in \mathbb{R}^n} \Psi(x) \quad \text{subject to} \quad \frac{1}{2} \|s(x) - b\|^2 = \frac{\sigma^2}{2}. \quad (3)$$

Here, the constraint expresses the discrepancy principle [2], which basically says that a point  $x$  that satisfies  $\|s(x) - b\| < \sigma$  is expected to be ‘over-fitted’ to the noisy data  $b$ .

Among all possible solutions  $x$  that fit data  $b$  ‘well enough’ without being over-fitted, the one that minimizes the regularization function  $\Psi(x)$  is chosen.

In this work we consider a computationally efficient approach to compute a solution  $(x^*, \lambda^*)$  to the nonlinear system of equations (2) by solving a sequence of sub-problems, by using the linear approximation  $s(x+p) \approx s(x) + J(x)p$  for the constraint in (3) for some  $x \in \mathbb{R}^n$ . By Taylor’s theorem we have

$$s(x+p) = s(x) + \int_0^1 J(x+tp)p dt.$$

Hence it follows that

$$\begin{aligned} \|s(x) + J(x)p - s(x+p)\| &= \|J(x)p - \int_0^1 J(x+tp)p dt\| \\ &= \left\| \int_0^1 (J(x) - J(x+tp)) p dt \right\| \\ &\leq \|p\| \max_{t \in [0,1]} \|J(x) - J(x+tp)\| = o(\|p\|). \end{aligned}$$

In case we assume that  $J(x)$  is Lipschitz continuous we get  $\mathcal{O}(\|p\|^2)$ .

From a small calculation it follows that we have the following equivalent expressions:

$$\frac{1}{2} \|J(x)p + s(x) - b\|^2 = \frac{\sigma^2}{2} \Leftrightarrow c(x) + \nabla c(x)^T p + \frac{1}{2} p^T J(x)^T J(x) p = 0.$$

Hence it is clear that taking a linear approximation of the forward model  $s(x+p)$  corresponds to taking a quadratic model of the constraint function  $c(x+p)$ . Alternatively we could have immediately considered a quadratic model of  $c(x+p)$  using Taylor’s theorem:

$$c(x+p) \approx c(x) + \nabla c(x)^T p + \frac{1}{2} p^T \nabla^2 c(x) p.$$

However, since  $c(x)$  is in general non-convex we have that the hessian is possibly indefinite, which is undesirable for optimization algorithms. Moreover, for a least squares function we know that the matrix  $J(x)^T J(x)$  is an approximation of the true hessian  $\nabla^2 c(x)$ . This approximation is for instance used in the Gauss-Newton algorithm [1] for solving a least squares minimization problem.

The main idea of the method proposed in this manuscript is to solve a sequence of problems of the form

$$\min_{p \in \mathbb{R}^n} \Psi(x+p) \quad \text{subject to} \quad \frac{1}{2} \|J(x)p + s(x) - b\|^2 = \frac{\sigma^2}{2} \quad (4)$$

for a given iterate  $x \in \mathbb{R}^n$ . The KKT conditions for this optimization problem are given by

$$\begin{cases} \nabla \Psi(x+p) + \lambda(\nabla c(x) + J(x)^T J(x)p) = 0, & (5a) \\ c(x) + \nabla c(x)^T p + \frac{1}{2} p^T J(x)^T J(x) p = 0, & (5b) \end{cases}$$

where  $\lambda \in \mathbb{R}$  is the Lagrange multiplier.

Alternatively, we could also consider a quadratic model of the objective function and solve a sequence of problems

$$\min_{p \in \mathbb{R}^n} \nabla \Psi(x)^T p + \frac{1}{2} p^T \nabla^2 \Psi(x) p \quad \text{subject to} \quad \frac{1}{2} \|J(x)p + s(x) - b\|^2 = \frac{\sigma^2}{2}. \quad (6)$$

In this case we would get an approach that closely resembles the one taken in [3], namely the Sequential Quadratically Constrained Quadratic programming (SQCQP) method. The SQCQP method is slightly more general in the sense that they work with possibly multiple constraint functions  $c_i(x) : \mathbb{R}^n \rightarrow \mathbb{R}$  for  $i = 1, \dots, m$ . However, they assume convexity of these functions and then use the true Hessians  $\nabla^2 c_i(x)$  in the quadratic model. With the numerical experiments, see section 4, it will become clear that in the context of the current manuscript it is better to solve a sequence of problems of the form (4). Hence, we focus our presentation on this case. However, many of the results presented here can be modified in case we solve a sequence of problems (6).

Note that even when (2) has a solution, this does not necessarily imply that (5) has a solution for all  $x$ . However, using the implicit function theorem, we can show that this sub-problem has a solution for all  $x$  in a neighborhood of the solution  $x^*$ . The implicit function theorem can be formulated as follows:

**Theorem 1.2.** *Let  $\Phi : \mathbb{R}^n \times \mathbb{R}^q \rightarrow \mathbb{R}^q$  be a continuously differentiable function and let  $\mathbb{R}^n \times \mathbb{R}^q$  have coordinates  $(x, y)$ . Suppose  $(x^*, y^*)$  is a point satisfying  $\Phi(x^*, y^*) = 0$ . If the Jacobian matrix of  $\Phi$  with respect to  $y$  is nonsingular in  $(x^*, y^*)$ , i.e. if the matrix  $J_\Phi(x^*, y^*) := \left( \frac{\partial \Phi_i(x^*, y^*)}{\partial y_j} \right)_{i,j} \in \mathbb{R}^{q \times q}$  is invertible, then there exists some open set  $X \subset \mathbb{R}^n$  containing  $x^*$  such that there exists a unique continuously differentiable function  $g : X \rightarrow \mathbb{R}^q$  such that  $g(x^*) = y^*$  and  $\Phi(x, g(x)) = 0$  for all  $x \in X$ .*

*Proof.* See for instance [4, 5]. □

**Lemma 1.3.** *Let  $(x^*, \lambda^*)$  be a KKT point (2) with  $\nabla c(x^*) \neq 0$  and suppose the matrix  $\nabla^2 \Psi(x^*) + \lambda^* J(x^*) J(x^*)^T$  is positive definite. Then there exist an open ball  $\mathcal{B}_\rho(x^*)$  with center  $x^*$  and radius  $\rho > 0$  such that for all  $x \in \mathcal{B}_\rho(x^*)$  there exists a solution  $(p, \lambda)$  for (5) with  $\lambda > 0$ .*

*Proof.* To prove this claim we apply the implicit function theorem to the function  $\Phi : \mathbb{R}^n \times \mathbb{R}^{n+1} \rightarrow \mathbb{R}^{n+1}$  with

$$\Phi(x, p, \lambda) = \begin{pmatrix} \nabla \Psi(x + p) + \lambda \nabla c(x) + \lambda J(x)^T J(x) p \\ c(x) + \nabla c(x)^T p + \frac{1}{2} p^T J(x)^T J(x) p \end{pmatrix}.$$

Obviously we have  $\Phi(x^*, 0, \lambda^*) = 0$  since  $(x^*, \lambda^*)$  solves (2). Moreover we have that the Jacobian of  $\Phi(x, p, \lambda)$  with respect to  $(p, \lambda)$  is given by

$$J_\Phi(x, p, \lambda) = \begin{pmatrix} \nabla^2 \Psi(x + p) + \lambda J(x)^T J(x) & J(x)^T J(x) p + \nabla c(x) \\ p^T J(x)^T J(x) + \nabla c(x)^T & 0 \end{pmatrix}.$$

Evaluating this matrix in  $(x^*, 0, \lambda^*)$  gives us

$$J_{\Phi}(x^*, 0, \lambda^*) = \begin{pmatrix} \nabla^2 \Psi(x^*) + \lambda^* J(x^*)^T J(x^*) & \nabla c(x^*) \\ \nabla c(x^*)^T & 0 \end{pmatrix} \quad (7)$$

which is non-singular since  $\nabla^2 \Psi(x^*) + \lambda^* J(x^*)^T J(x^*)$  is positive definite and  $\nabla c(x^*) \neq 0$ . Hence, from theorem 1.2 it follows that there exists an open set  $X \subset \mathbb{R}^n$  containing  $x^*$  such that there exists a unique continuously differentiable function  $g : X \rightarrow \mathbb{R}^{n+1}$  such that  $g(x^*) = (0, \lambda^*)$  and  $\Phi(x, g(x)) = 0$  for all  $x \in X$ . It is now clear that  $g(x) = (p, \lambda)$  is a solution for (5). Furthermore, by continuity of  $g(x)$  and the fact that  $\lambda^* > 0$  we can choose the any radius  $\rho > 0$  small enough such that  $\mathcal{B}_{\rho}(x^*) \subset X$  and  $\lambda > 0$ .  $\square$

The rest of the paper is organized as follows. In section 2 we derive the Sequential Projected Newton method, which is based on (approximately) solving a sequence of problems of the form (4). Next, in section 3, we introduce the application that we consider for our numerical experiments, namely Talbot-Lau x-ray phase contrast imaging. In section 4 we perform a number of experiments with the newly proposed algorithm and illustrate its effectiveness in solving the nonlinear inverse problem. Lastly this work is concluded in section 5.

## 2. Derivation of the Sequential Projected Newton method

In this section we describe a line-search strategy that can be used when solving a sequence of problems of the form (5). Let us first describe a good choice of initial point  $x_0$  to start our algorithm. We know that there exists a point  $x_0$  that satisfies  $\|s(x_0) - b\| \leq \sigma$ , since we assumed that the unconstrained solution is below the noise-level. Moreover, such a point can be computed very easily by performing just a few Gauss-Newton iterations applied to  $\operatorname{argmin}_{x \in \mathbb{R}^n} \|s(x) - b\|$ . For such a point we know that the linearized inequality constraint  $\|J(x_0)p + s(x_0) - b\| \leq \sigma$  is feasible, since  $p = 0$  satisfies the inequality. From this it follows that the equality constraint  $\|J(x_0)p + s(x_0) - b\| = \sigma$  is also feasible, since the constraint function  $c(x)$  can be seen as a convex paraboloid. This means that the nonlinear system of equations (5) has a solution for  $x = x_0$  and hence we can use this as our initial point.

Let us denote  $[\cdot]^+ = \max\{0, \cdot\}$ . It is well known that the following function is an exact merit function for the optimization problem (1):

$$F_r(x) = \Psi(x) + r[c(x)]^+.$$

The authors in [3] use this merit function in proving global convergence of the SQCQP method. The analysis in this section is inspired by this work.

In this section we will show that if we choose the penalty parameter  $r > 0$  large enough, we can then always find a step-length  $\beta \in (0, 1]$  such that  $F_r(x + \beta p) < F_r(x)$ . We start by proving the following lemma:

**Lemma 2.1.** For all  $x \in \mathcal{B}_\rho(x^*)$  there exists a constant  $\phi > 0$  such that

$$\Psi(x + \beta p) - \Psi(x) \leq -\frac{\beta\lambda}{2} p^T J(x)^T J(x) p + \lambda\beta c(x) + \phi\beta^2 \|p\|^2$$

where  $(p, \lambda)$  is the KKT pair (5).

*Proof.* By Taylor's theorem we have that there exists some  $t_\beta \in (0, 1)$  such that

$$\Psi(x + \beta p) = \Psi(x) + \beta \nabla \Psi(x)^T p + \frac{\beta^2}{2} p^T \nabla^2 \Psi(x + t_\beta \beta p) p$$

and thus we have for all  $\beta$  that

$$\Psi(x + \beta p) - \Psi(x) \leq \beta \nabla \Psi(x)^T p + \phi\beta^2 \|p\|^2 \quad (8)$$

with  $\phi = \max_{t \in (0, 1)} \frac{1}{2} \|\nabla^2 \Psi(x + tp)\|$ . Moreover, we also have

$$\nabla \Psi(x + p) = \nabla \Psi(x) + \int_0^1 \nabla^2 \Psi(x + tp) p dt$$

which implies  $\nabla \Psi(x)^T p \leq \nabla \Psi(x + p)^T p$  since  $\nabla^2 \Psi(x)$  is positive semi-definite. Using this inequality together with (8) and the KKT conditions (5), we get

$$\begin{aligned} \Psi(x + \beta p) - \Psi(x) &\leq \beta \nabla \Psi(x + p)^T p + \phi\beta^2 \|p\|^2 \\ &= \lambda\beta (-\nabla c(x)^T p - p^T J(x)^T J(x) p) + \phi\beta^2 \|p\|^2 \\ &= \lambda\beta c(x) - \frac{\beta\lambda}{2} p^T J(x)^T J(x) p + \phi\beta^2 \|p\|^2. \end{aligned}$$

□

**Lemma 2.2.** Let  $x \in \mathcal{B}_\rho(x^*)$  with corresponding KKT pair  $(p, \lambda)$  that satisfies (5) and  $r > \lambda$ . Let  $0 < \eta < 1$ , then we have for all  $\beta$  sufficiently small

$$F_r(x + \beta p) - F_r(x) \leq -\frac{\eta\lambda\beta}{2} p^T J(x)^T J(x) p. \quad (9)$$

*Proof.* From lemma 2.1 we have that there exists a constant  $\phi_1 > 0$  such that

$$\Psi(x + \beta p) - \Psi(x) \leq -\frac{\beta\lambda}{2} p^T J(x)^T J(x) p + \lambda\beta c(x) + \phi_1\beta^2 \|p\|^2.$$

From the second equation in (5) it follows that  $c(x) + \nabla c(x)^T p \leq 0$ . Hence, for all  $\beta \in [0, 1]$  we have

$$c(x) + \beta \nabla c(x)^T p \leq (1 - \beta)c(x).$$

From this it also follows that

$$[c(x) + \beta \nabla c(x)^T p]^+ - [c(x)]^+ \leq -\beta [c(x)]^+.$$

Again using Taylor's theorem we have for some  $t_\beta \in (0, 1)$  that

$$\begin{aligned} [c(x + \beta p)]^+ &= \left[ c(x) + \beta \nabla c(x)^T p + \frac{\beta^2}{2} p^T \nabla^2 c^2(x + t_\beta \beta p) p \right]^+ \\ &\leq [c(x) + \beta \nabla c(x)^T p]^+ + \left[ \frac{\beta^2}{2} p^T \nabla^2 c^2(x + t_\beta \beta p) p \right]^+ \\ &\leq [c(x) + \beta \nabla c(x)^T p]^+ + \phi_2 \beta^2 \|p\|^2 \end{aligned}$$

with  $\phi_2 = \max_{t \in (0,1)} \frac{1}{2} \|\nabla^2 c(x + tp)\|$ . As a consequence we also have

$$\begin{aligned} [c(x + \beta p)]^+ - [c(x)]^+ &\leq [c(x) + \beta \nabla c(x)^T p]^+ - [c(x)]^+ + \phi_2 \beta^2 \|p\|^2 \\ &\leq -\beta [c(x)]^+ + \phi_2 \beta^2 \|p\|^2 \end{aligned}$$

Let us now write

$$\begin{aligned} F_r(x + \beta p) - F_r(x) &= \Psi(x + \beta p) - \Psi(x) + r ([c(x + \beta p)]^+ - [c(x)]^+) \\ &\leq -\frac{\beta \lambda}{2} p^T J(x)^T J(x) p + \lambda \beta c(x) + \phi_1 \beta^2 \|p\|^2 - r \beta [c(x)]^+ + r \phi_2 \beta^2 \|p\|^2 \\ &\leq -\frac{\beta \lambda}{2} p^T J(x)^T J(x) p + \beta (\lambda - r) [c(x)]^+ + (\phi_1 + r \phi_2) \beta^2 \|p\|^2 \\ &\leq -\frac{\beta \lambda}{2} p^T J(x)^T J(x) p + (\phi_1 + r \phi_2) \beta^2 \|p\|^2 \end{aligned}$$

The final inequality follows from the fact that  $r > \lambda$ . It is clear that (9) holds for all values of  $\beta$  that satisfy

$$-\frac{\beta \lambda}{2} p^T J(x)^T J(x) p + (\phi_1 + r \phi_2) \beta^2 \|p\|^2 \leq -\frac{\eta \lambda \beta}{2} p^T J(x)^T J(x) p$$

By rearranging the terms it follows that the above equality holds for all  $\beta$  with

$$\beta \leq \frac{(1 - \eta) \lambda p^T J(x)^T J(x) p}{2(\phi_1 + r \phi_2) \|p\|^2}.$$

This concludes the proof since the right-hand side in this equality is strictly positive.  $\square$

**Theorem 2.3.** *Suppose we generate an infinite sequence of iterates  $x_k = x_{k-1} + \beta_k p_k$  that all satisfy descent condition (9) for penalty parameter  $r_k = \max(2\lambda_k, r_{k-1})$ , with  $(p_k, \lambda_k)$  the KKT pair (5) corresponding with  $x_{k-1}$  and  $r_0$  an initial penalty parameter. Suppose  $J(x_{k-1})^T J(x_{k-1}) \succeq \mu I$  for some constant  $\mu > 0$  independent of  $k$ . Suppose in addition that the iterates  $(x_k, \lambda_k)$  remain bounded and that there exists a constant  $\gamma$  independent of  $k$  such that  $\beta_k \lambda_k > \gamma > 0$ . Then there exists a sub-sequence  $\mathcal{K} \subset \mathbb{N}$  such that  $(x_k, \lambda_k)_{k \in \mathcal{K}}$  converges to a solution of (2).*

*Proof.* By boundedness of  $(x_k, \lambda_k)$  we know, using the Bolzano-Weierstrass theorem, that there exist a convergent sub-sequence  $(x_k, \lambda_k)_{k \in \mathcal{K}} \rightarrow (\bar{x}, \bar{\lambda})$  for some  $\mathcal{K} \subset \mathbb{N}$ . Hence,

we can assume that  $r_k = r$  for some constant  $r$  for all  $k \in \mathcal{K}$  sufficiently large. Since the descent condition (9) holds and  $\lambda_k \beta_k > \gamma$  we have for  $k$  sufficiently large

$$F_r(x_k) - F_r(x_{k-1}) \leq -\frac{\eta \lambda_k \beta_k}{2} p_k^T J(x_{k-1})^T J(x_{k-1}) p_k \leq -\frac{\eta \mu \gamma}{2} \|p_k\|^2.$$

In addition we have that the sequence  $F_r(x_k)$  is decreasing and bounded below and thus it must converge. Hence, it also follows that  $F_r(x_{k-1}) - F_r(x_k) \rightarrow 0$ . Combining this with the fact that  $F_r(x_{k-1}) - F_r(x_k) \geq \frac{\eta \mu \gamma}{2} \|p_k\|^2$ , we can conclude that  $p_k \rightarrow 0$ . Writing out the KKT conditions (5) for  $(x_k, \lambda_k)$  we get

$$\begin{cases} \nabla \Psi(x_k + p_k) + \lambda_k (\nabla c(x_k) + J(x_k)^T J(x_k) p_k) = 0, \\ c(x_k) + \nabla c(x_k)^T p_k + \frac{1}{2} p_k^T J(x_k)^T J(x_k) p_k = 0. \end{cases}$$

Now by taking the limit for  $k \in \mathcal{K}$  and using the fact that  $p_k \rightarrow 0$  we have

$$\begin{cases} \nabla \Psi(\bar{x}) + \bar{\lambda} \nabla c(\bar{x}) = 0, \\ c(\bar{x}) = 0, \end{cases}$$

which concludes the proof.  $\square$

The results above allow us to formulate a line-search method for solving (2), see algorithm 1. Convergence of the algorithm can be monitored using the nonlinear function

$$F(x, \lambda) = \begin{pmatrix} \nabla \Psi(x) + \lambda \nabla c(x) \\ c(x) \end{pmatrix} \quad (10)$$

that expresses the KKT conditions (2) of the equality constrained optimization problem (3) (not to be confused with the merit function  $F_r(x)$  used in the line-search). In section 4 we also investigate other possible convergence metrics.

---

**Algorithm 1** “exact” Sequential Projected Newton method (exact SPN)

---

- 1: Initialize  $k = 0$ ,  $r_0 > 0$  and  $\eta, \theta \in (0, 1)$  and choose tolerance  $\tau$ .
- 2: Compute initial point  $x_0$  with  $\|s(x_0) - b\| \leq \sigma$  and set  $\lambda_0 = -\frac{\nabla \Psi(x_0)^T \nabla c(x_0)}{\|\nabla c(x_0)\|^2}$ .
- 3: **while**  $\|F(x_k, \lambda_k)\| \geq \tau$  **do**
- 4:   Solve (5) for  $x = x_k$  and denote the solution as  $(p_{k+1}, \tilde{\lambda}_{k+1})$ .
- 5:   Update penalty parameter  $r_{k+1} = \max(2\tilde{\lambda}_{k+1}, r_k)$ .
- 6:   Choose  $\beta_{k+1}$  the largest value in  $\{1, \theta, \theta^2, \theta^3, \dots\}$  such that

$$F_{r_{k+1}}(x_k + \beta_{k+1} p_{k+1}) - F_{r_{k+1}}(x_k) \leq -\frac{\eta \tilde{\lambda}_{k+1} \beta_{k+1}}{2} \|J(x_k) p_{k+1}\|^2$$

- 7:   Update  $x_{k+1} = x_k + \beta_{k+1} p_{k+1}$  and  $\lambda_{k+1} = \lambda_k + \beta_{k+1} (\tilde{\lambda}_{k+1} - \lambda_k)$ .
  - 8:    $k = k + 1$
  - 9: **end while**
-

Note that the definition of  $\lambda_0$  on line 2 can be seen as the least squares approximation of the Lagrange multiplier corresponding with  $x_0$ , see for instance [6]. First of all by lemma 2.2 we have that the backtracking line-search on line 6 is well-defined and terminates with some  $\beta_{k+1} > 0$ . Furthermore we know by theorem 2.3 that this algorithm converges towards the solution of (2) under certain assumptions. We acknowledge that the assumptions in theorem 2.3 – although very often satisfied in practice – are relatively crude. However, we have no real interest in loosening these assumptions since, for practical purposes which will become clear in the rest of the manuscript, we need to consider a slightly more heuristic formulation of algorithm 1 that significantly improves the computational cost of the algorithm.

Let us explain this in a bit more detail. In principle we can use any constrained optimization algorithm to solve (4) on line 4. However, the Projected Newton (PN) method [7] is particularly well suited to solve this problem, since it exploits some of the problem-specific properties. The Projected Newton method is itself an iterative method that uses Generalized Krylov subspaces to solve a sequence of projected problems. The number of floating point operations used in the Projected Newton method grows with the iteration index of the algorithm, so for performance it is important that the number of iterations required to converge remains relatively small. Hence, if we require that (4) is solved very accurately, then algorithm 1 will not be very efficient. In the numerical experiments section we illustrate that (4) does not have to be solved very accurately to be able to make progress towards the solution. Furthermore it turns out that (4) is a very accurate model of (3) in the sense that the descent property (9) is satisfied by  $\beta = 1$  for all iterations in the experiments of section 4. Hence, to improve performance of the algorithm and remove the seemingly unnecessary line-search we describe a slightly more heuristic approach.

To formulate the computationally efficient variant of algorithm 1 we define

$$F^{(k)}(p, \lambda) = \begin{pmatrix} \nabla\Psi(x_k + p) + \lambda (\nabla c(x_k) + J(x_k)^T J(x_k)p) \\ c(x_k) + \nabla c(x_k)^T p + \frac{1}{2} p^T J(x_k)^T J(x_k)p \end{pmatrix} \quad (11)$$

the system of non-linear equations that express the KKT conditions (5) of the sub-problem on line 4 of algorithm 1 for  $x = x_k$ . Algorithm 2 is a heuristic approach that works very well in practice. We illustrate this claim by a number of numerical experiments in section 4.

### 3. Test problem: Talbot-Lau x-ray phase contrast imaging

For our numerical experiments we consider a test-problem from Talbot-Lau phase contrast imaging [8]. The forward model of the Talbot-Lau phase contrast projection operation in the discretized setting can be described with:

$$s(\mu, \epsilon, \delta) = s_0 e^{-A\mu} [1 + v_0 e^{-A\epsilon} \cos(\phi_0 + A_\phi \delta)] \quad (13)$$

**Algorithm 2** Sequential Projected Newton method

- 
- 1: Initialize  $k = 0$  and  $\zeta > 1$  and choose tolerance  $\tau$ .
  - 2: Compute initial point  $x_0$  with  $\|s(x_0) - b\| \leq \sigma$  and set  $\lambda_0 = -\frac{\nabla\Psi(x_0)^T \nabla c(x_0)}{\|\nabla c(x_0)\|^2}$ .
  - 3: **while**  $\|F(x_k, \lambda_k)\| \geq \tau$  **do**
  - 4:   Apply Projected Newton method to

$$\min_{p \in \mathbb{R}^n} \Psi(x_k + p) \quad \text{subject to} \quad \frac{1}{2} \|J(x_k)p + s(x_k) - b\|^2 = \frac{\sigma^2}{2} \quad (12)$$

with stopping criterion  $\|F^{(k)}(p_{k+1}, \lambda_{k+1})\| \leq \max \left\{ \frac{\|F(x_k, \lambda_k)\|}{\zeta}, \tau \right\}$

- 5:   Update  $x_{k+1} = x_k + p_{k+1}$
  - 6:    $k = k + 1$
  - 7: **end while**
- 

where  $s_0 \in \mathbb{R}_0^+$  is the incoming intensity,  $v_0 \in (0, 1)$  the visibility and  $\phi_0 \in \mathbb{R}^m$  the phase shift without the object. The variables  $\mu, \epsilon$  and  $\delta$  are the absorption, dark field and phase contrast, respectively. In the current manuscript we consider two-dimensional examples where the three components  $\mu, \epsilon$  and  $\delta$  can be visualized as pixel images. Similarly we could also consider three dimensional examples where the different components contain a large number of voxels. If we denote  $\tilde{n}$  the total number of pixels (or voxels) then we have  $\mu, \epsilon, \delta \in \mathbb{R}^{\tilde{n}}$ . Now let  $m$  denote the total number of projections, i.e. the number of projection angles times the number of detectors. Then we have  $s(\mu, \epsilon, \delta) \in \mathbb{R}^m$ . In addition, we denote  $b$  the vector of length  $m$  containing the acquired (noisy) projections.

The matrix  $A \in \mathbb{R}^{m \times \tilde{n}}$  is the conventional projection matrix and  $A_\phi \in \mathbb{R}^{m \times \tilde{n}}$  the system matrix for differential phase contrast:  $A_\phi = DA$ , where  $D \in \mathbb{R}^{m \times m}$  is a matrix performing the finite difference operation. We generate the matrix  $A$  using the ASTRA toolbox [9, 10] based on a simple parallel beam geometry with line kernel, see Appendix A. Let us denote  $x = [\mu^T, \epsilon^T, \delta^T]^T \in \mathbb{R}^n$  with  $n = 3\tilde{n}$  the vector obtained by stacking the three components. Note that  $s_i(x)$  is a function  $\mathbb{R}^n \rightarrow \mathbb{R}$  and  $s(x)$  is a function  $\mathbb{R}^n \rightarrow \mathbb{R}^m$ .

To use the techniques developed in this manuscript we first need to compute the Jacobian matrix  $J(x)$  of the nonlinear forward model  $s(x)$ . To do so it is convenient to write  $s(x) = \tilde{s}(\tilde{x})$ , with  $\tilde{x} = \bar{A}x = [t^T, u^T, v^T]^T \in \mathbb{R}^{3m}$ ,

$$\bar{A} = \begin{pmatrix} A & 0 & 0 \\ 0 & A & 0 \\ 0 & 0 & A_\phi \end{pmatrix} \quad \text{and} \quad \tilde{s}_i(\tilde{x}) = s_0 e^{-t_i} [1 + v_0 e^{-u_i} \cos(\phi_0 + v_i)], \quad (i = 1, \dots, m).$$

Let us calculate the Jacobian  $J_{\tilde{s}}(\tilde{x})$  of the function  $\tilde{s}(\tilde{x})$ . For  $i \neq j$  we have that  $\frac{\partial \tilde{s}_i}{\partial t_j} = \frac{\partial \tilde{s}_i}{\partial u_j} = \frac{\partial \tilde{s}_i}{\partial v_j} = 0$  and for  $i = j$  we have

$$\frac{\partial \tilde{s}_i}{\partial t_i} = -\tilde{s}_i, \quad \frac{\partial \tilde{s}_i}{\partial u_i} = -s_0 v_0 e^{-t_i} e^{-u_i} \cos(\phi_0 + v_i) \quad \text{and} \quad \frac{\partial \tilde{s}_i}{\partial v_i} = -s_0 v_0 e^{-t_i} e^{-u_i} \sin(\phi_0 + v_i).$$

Hence we can write  $J_{\tilde{s}}(\tilde{x}) = \begin{pmatrix} -D_1(\tilde{x}) & -D_2(\tilde{x}) & -D_3(\tilde{x}) \end{pmatrix} \in \mathbb{R}^{m \times 3m}$  with

$$\begin{aligned} D_1(\tilde{x}) &= \text{diag}(\tilde{s}_i)_{i=1,\dots,m} \\ D_2(\tilde{x}) &= \text{diag}(s_0 v_0 e^{-t_i} e^{-u_i} \cos(\phi_0 + v_i))_{i=1,\dots,m} \\ D_3(\tilde{x}) &= \text{diag}(s_0 v_0 e^{-t_i} e^{-u_i} \sin(\phi_0 + v_i))_{i=1,\dots,m}. \end{aligned}$$

Using the chain rule for the Jacobian  $s(x) = \tilde{s}(\bar{A}x)$  we immediately get

$$J(x) = J_{\tilde{s}}(\bar{A}x)\bar{A} = \begin{pmatrix} -D_1(\bar{A}x)A & -D_2(\bar{A}x)A & -D_3(\bar{A}x)A \end{pmatrix}.$$

### 3.1. Total variation regularization

Total variation regularization is a popular regularization technique that preserves edges in images. Let  $y \in \mathbb{R}^{\tilde{n}}$  be a vector obtained by stacking all columns of a pixel image  $Y \in \mathbb{R}^{N \times N}$  with  $\tilde{n} = N^2$ . The anisotropic total variation function is defined as

$$\text{TV}(y) = \sum_{i,j=1}^N |\partial_h^{(i,j)}(Y)| + |\partial_v^{(i,j)}(Y)|. \quad (14)$$

with finite difference operators in the horizontal and vertical direction given by

$$\partial_h^{(i,j)}(Y) = \begin{cases} Y_{i,j+1} - Y_{i,j} & j < N \\ 0 & j = N \end{cases} \quad \text{and} \quad \partial_v^{(i,j)}(Y) = \begin{cases} Y_{i+1,j} - Y_{i,j} & i < N \\ 0 & i = N \end{cases}.$$

We can rewrite this in a more convenient way by first writing

$$\tilde{D} = \begin{pmatrix} 1 & -1 & & \\ & \ddots & \ddots & \\ & & 1 & -1 \end{pmatrix} \in \mathbb{R}^{(N-1) \times N}$$

which represents a finite difference approximation of the derivative operator in one dimension. Let  $\otimes$  denote the Kronecker product. We can compactly write  $\text{TV}(y) = \|\tilde{L}y\|_1$  with

$$\tilde{L} = \begin{pmatrix} D_h \\ D_v \end{pmatrix} \in \mathbb{R}^{(2\tilde{n}-2N) \times \tilde{n}} \quad \text{and} \quad \begin{cases} D_h = \tilde{D} \otimes I_N \in \mathbb{R}^{(\tilde{n}-N) \times \tilde{n}} \\ D_v = I_N \otimes \tilde{D} \in \mathbb{R}^{(\tilde{n}-N) \times \tilde{n}} \end{cases}. \quad (15)$$

The matrices  $D_h$  and  $D_v$  represent the two dimensional finite difference approximation of the derivative operator in the horizontal and the vertical directions respectively. Now because we have three different images  $\mu, \epsilon$  and  $\delta$  we consider the regularization term  $\|Lx\|_1$  with

$$L = \begin{pmatrix} \tilde{L} & 0 & 0 \\ 0 & \tilde{L} & 0 \\ 0 & 0 & \tilde{L} \end{pmatrix} \in \mathbb{R}^{\tilde{m} \times n} \quad (16)$$

and  $\tilde{m} = 3(2\tilde{n} - 2N)$ . The  $\ell_1$  norm is of course non-differentiable, however, it is easy to formulate a smooth approximation  $\Psi(x) \approx \|Lx\|_1$ , where  $\Psi : \mathbb{R}^n \rightarrow \mathbb{R}$  is a twice continuously differentiable convex function. More precisely we define

$$\Psi(x) = \sum_{i=1}^{\tilde{m}} \sqrt{[Lx]_i^2 + \xi} \quad (17)$$

where  $\xi > 0$  is a small scalar that ensures smoothness. This is the same technique as used in [7].

#### 4. Numerical experiments

In this section we perform a number of numerical experiments using the Talbot-Lau test-problem described in section 3. The aim is to illustrate that algorithm 2 is a robust and computationally efficient method for solving the nonlinear system of equations  $F(x, \lambda) = 0$  defined by the KKT equations (10) for the equality constrained optimization problem (3). This function is also used to monitor convergence of the algorithm. The experiments are all performed using MATLAB R2017a.

For all our experiments we set  $s_0 = 1$  in the forward model (13), which can be seen as a normalization of the projection data. Unless explicitly stated otherwise, the value  $v_0 = 0.75$  is used for the visibility and  $\phi_0$  is generated using three phase steps. We refer to Appendix A for more details on how the test-problems are generated. For a certain exact solution  $x_{ex} = (\mu_{ex}, \epsilon_{ex}, \delta_{ex})$  we generate exact data  $b_{ex} = s(x_{ex})$  and then add Gaussian distributed white noise to obtain noisy data  $b$ . We refer to the value  $\sigma = \|b - b_{ex}\|$  as the noise-level and to  $\sigma/\|b_{ex}\|$  as the relative noise-level. We denote **npix** the number of pixels in each direction (we only consider square images) and **nangles** the number of projection angles used and we set the number of detectors equal to **npix**. For these choices we have  $n = 3 \times \text{npix}^2$  unknowns and  $m = \text{npix} \times \text{nangles}$  measurements. We always choose **nangles** to be a multiple ( $\geq 3$ ) of **npix**, which implies  $m \geq n$ . In each iteration of the SPN algorithm we start the Projected Newton method with initial Lagrange multiplier  $10^5$ , which works well in practice.

**Experiment 1.** We start by performing a small experiment with some exact images  $\mu_{ex}, \epsilon_{ex}$  and  $\delta_{ex}$  of size  $10 \times 10$ , i.e. **npix** = 10, and **nangles** =  $4 \times \text{npix}$ , resulting in a projection matrix  $A$  of size  $400 \times 100$ . Next we generate data  $b$  with relative noise-level 0.01 in MATLAB as follows

```

1 npix = 10; nangles = 4*npix, nstep = 3; v0 = 0.75; nn = npix^2;
2 x_ex = randn(3*nn,1)/10;
3 [A,D,phi0] = generate_testproblem(npix,nangles,nstep) %Appendix A.
4 b_ex = exp(-A*x_ex(1:nn)).* ...
    (1+v0*exp(-A*x_ex(nn+1:2*nn)).*cos(phi0+D*(A*x_ex(2*nn+1:end)))));
5 noiselevel = 0.01; noise = randn(m, 1);
6 b = b_ex + noiselevel*norm(b_ex)*noise/norm(noise);

```

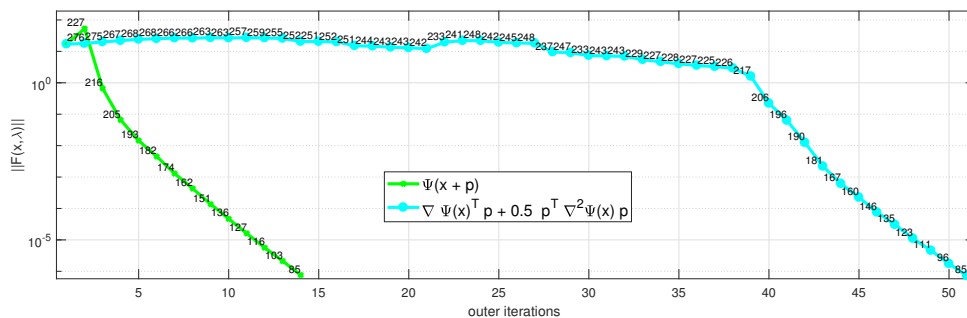


Figure 1: **Experiment 1.** Convergence history of algorithm 1 compared with the same algorithm where sub-problem (4) is replaced by the quadratic model (6). Full step-sizes  $\beta_k$  satisfy the decrease condition when we solve sub-problem (4), while smaller step-sizes are needed in case we use the quadratic model. The numbers reported on the figure are the number of inner iterations required for that particular outer iteration.

We apply the “exact” Sequential Projected Newton method, algorithm 1, with  $\Psi(x) = \sum_{i=1}^n \sqrt{x_i^2 + \xi}$  and parameters  $\eta = 10^{-4}$ ,  $\theta = 0.5$ ,  $\tau = 10^{-6}$  and  $\xi = 10^{-6}$ . Note that this choice of regularization term can be seen as a smooth approximation of the  $\ell_1$ -norm, which is not a good choice for the random exact solution that we generated above. However, with the current experiment we are not yet concerned with the quality of the obtained solution, but only with the convergence behavior.

For comparison we also apply a modified version of algorithm 1, where we replace sub-problem (4) on line 4 with sub-problem (6) that uses a quadratic model of  $\Psi(x+p)$ . As previously mentioned, we can readily modify the analysis in section 2 to show similar results for this modified version. In fact, the algorithm then closely resembles the SQCQP method developed in [3], for which the authors give a local and global convergence analysis. We use the Projected Newton method [7] to solve both these sub-problems and set the tolerance for this solver to  $\tau/10$ , i.e. we stop the algorithm when we have found a point that satisfies  $\|F^{(k)}(p_{k+1}, \tilde{\lambda}_{k+1})\| \leq \tau/10$ , where  $F^{(k)}(p, \lambda)$  is defined by (11).

The result of this experiment is given by figure 1. We compare the value  $\|F(x_k, \lambda_k)\|$  for both methods in terms of the outer SPN iterations  $k$ . In addition we also report the number of inner Projected Newton iterations required to converge for the sub-problems. First of all it is important to note that the decrease condition on line 6 is satisfied by the step-length  $\beta_k = 1$  for all iterations  $k$  in case we solve sub-problem (4). In contrast, in case we use a quadratic model (6), the line-search terminates with  $\beta_k < 1$  for a large number of iterations. This is the reason that the convergence in the latter case is much slower. It is also interesting to observe that the quadratic model requires more Projected Newton iterations on average to satisfy the stopping criterion. Hence it is clear from this experiment why choosing sub-problem (4) over (6) is the better choice.

**Experiment 2.** In the next experiment we illustrate the fact that the sub-problem

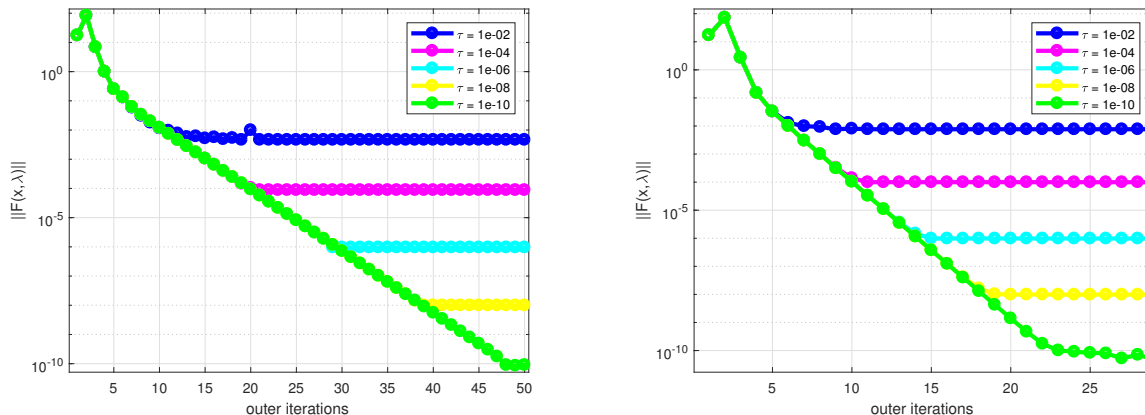


Figure 2: **Experiment 2.** Influence of the tolerance of the Projected Newton inner-solver on the convergence history in term of outer iterations of the Sequential Projected Newton method for two test-problems with different relative noise-level 0.1 (left) and 0.01 (right).

(4) does not have to be solved to a high accuracy to be able to make progress towards the solution, i.e. to decrease  $\|F(x, \lambda)\|$ . We keep the same set-up as before and consider two different relative noise-levels, namely 0.1 and 0.01. We apply algorithm 2 with  $\zeta = \infty$  and  $\tau = 10^{-4}, 10^{-6}, 10^{-8}$  and  $10^{-10}$ . This can be seen as applying algorithm 1, i.e. taking a fixed tolerance for the sub-problems, but always taking a full step-length (which satisfy the decrease condition on line 6 anyway). To clearly observe the effect of the tolerance of the Projected Newton method on convergence, we let the algorithm run for a fixed number of iterations. The result of this experiment is given by figure 2. The final achievable accuracy in terms of  $\|F(x, \lambda)\|$  is completely determined by the tolerance of the inner-solver. Furthermore, it can be observed that convergence (up to stagnation of the method) does not differ much in case we use a lower tolerance for the sub-problems. This implies that in early iterations it is not necessary to compute a very accurate solution. Hence an adaptive tolerance as implemented using the  $\zeta$  coefficient in algorithm 2 seems like a good idea to improve performance of the algorithm. This is especially important since the computational cost of the Projected Newton method grows with the number of iterations. With the next experiment we investigate the trade-off between keeping the number of inner iterations as low as possible without compromising the convergence in terms of the number of outer iterations needed to converge.

**Experiment 3.** In this experiment we study the effect of the parameter  $\zeta > 1$  in algorithm 2. If this value is large, then we require a relatively accurate solution of the sub-problem and we can expect that we need a large number of inner iterations to converge. However, we can also expect to make significant progress towards the solution in terms of  $\|F(x_k, \lambda_k)\|$  for the outer iterations. To confirm this we apply the Sequential

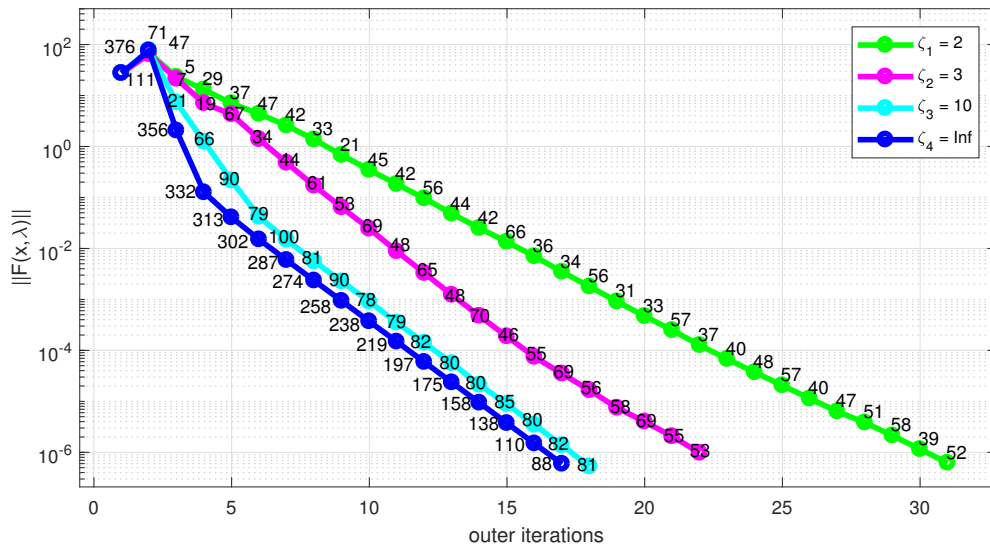


Figure 3: **Experiment 3.** Influence of the  $\zeta$  parameter on the convergence history of algorithm 2 in terms of the outer iterations. The numbers reported on the figure are the number of inner iterations required for that outer iteration.

Projected Newton method, algorithm 2, with different values of the  $\zeta$  parameter to a Talbot-Lau test-problem with `npix` = 16 and `nangles` =  $5 \times \text{npix}$ . Furthermore we take noise-level 0.01,  $v_0 = 0.5$ , tolerance  $\tau = 10^{-6}$  and smoothing parameter  $\xi = 10^{-6}$ .

In figure 3 we show convergence of the method for  $\zeta = 2, 3, 10$  and  $\infty$ . When we take a small value such as  $\zeta = 2$  we can observe that the number of inner iterations needed to satisfy the stopping criterion is relatively small. However, convergence in terms of the outer iterations is also quite slow. For the choice  $\zeta = \infty$  we get very rapid convergence in terms of outer iterations since we require an accurate solution ( $\tau = 10^{-6}$ ) of the sub-problem, but we need a lot inner iterations to satisfy the stopping criterion of the inner-solver. It is also interesting to observe that in this case the number of Projected Newton iteration decreases towards convergence. This is because the Projected Newton method starts from an initial point containing all zeroes and near the solution of  $F(x, \lambda) = 0$  we have that this is indeed a good initial “guess” for  $p_k$ . The choice  $\zeta = 10$  seems to nicely balance the effects we have for the other choices. Convergence of the outer iterations is comparable to that of the case  $\zeta = \infty$ , but a lot less inner iterations are required. This value is used in all subsequent experiments.

**Experiment 4.** For our final two experiments we turn our attention to the quality of the obtained solution when using total variation for the regularization function, as implemented in (17). We use the exact images for  $\mu_{ex}, \epsilon_{ex}$  and  $\delta_{ex}$  with `npix` = 64 as shown in figure 5 and we take `nangles` =  $5 \times \text{npix}$ , tolerance  $\tau = 10^{-6}$ , noiselevel 0.01,  $\zeta = 10$  and smoothing parameter  $\xi = 10^{-8}$ . Note that it is important that the smoothing parameter is relatively small, otherwise (17) is not a good approximation of

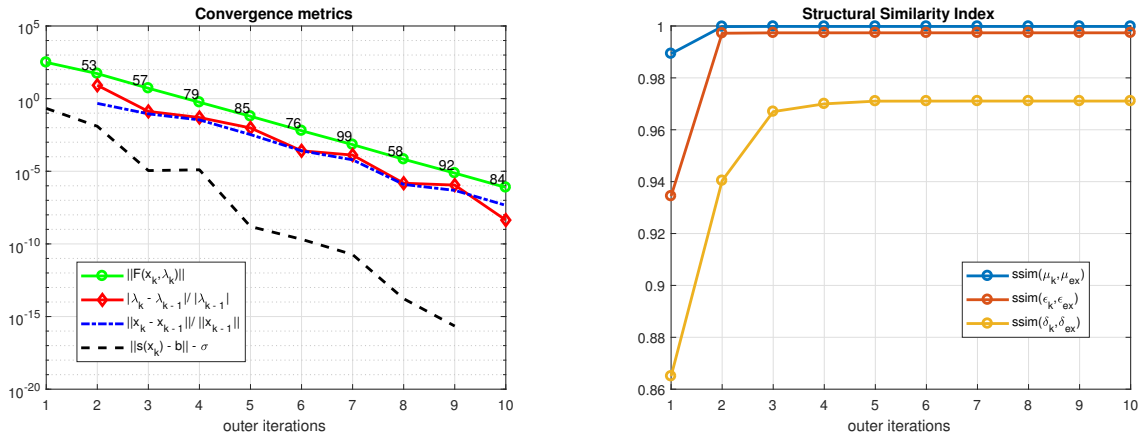


Figure 4: **Experiment 4.** (Left) Convergence metrics of a Talbot-Lau experiment with  $npix = 64$  and  $nangles = 5 \times npix$ . Tolerance is set to  $\tau = 10^{-3}$  and noiselevel 0.01. (Right) Structural Similarity index for the different components  $\mu_k$ ,  $\epsilon_k$  and  $\delta_k$  for the same experiment.

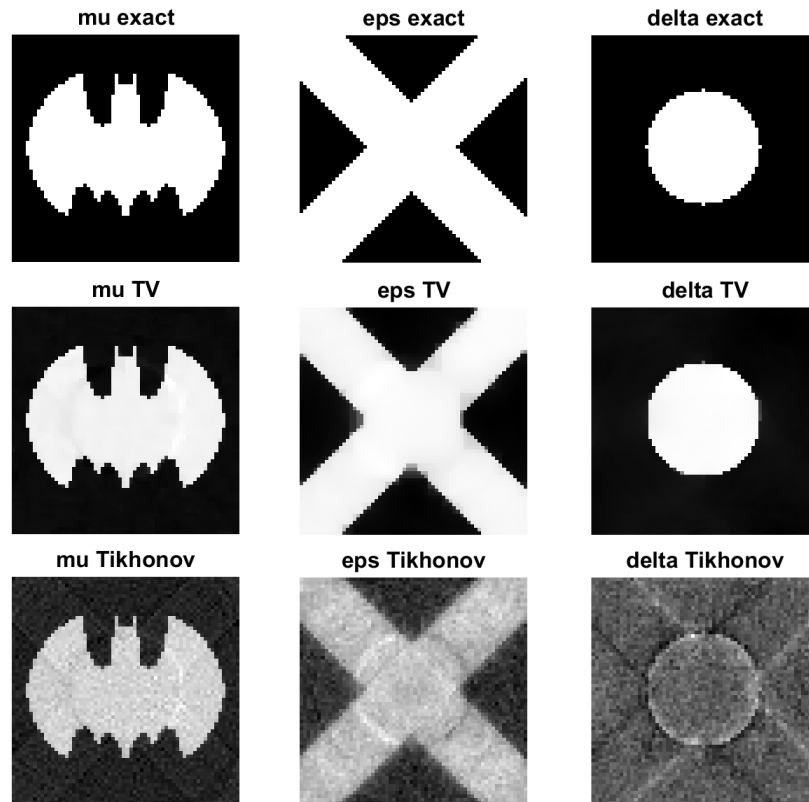


Figure 5: **Experiment 4.** The exact solution used in the experiment (top), the solution obtained by algorithm 2 with Total variation regularization (middle) and solution obtained using standard form Tikhonov regularization (bottom).

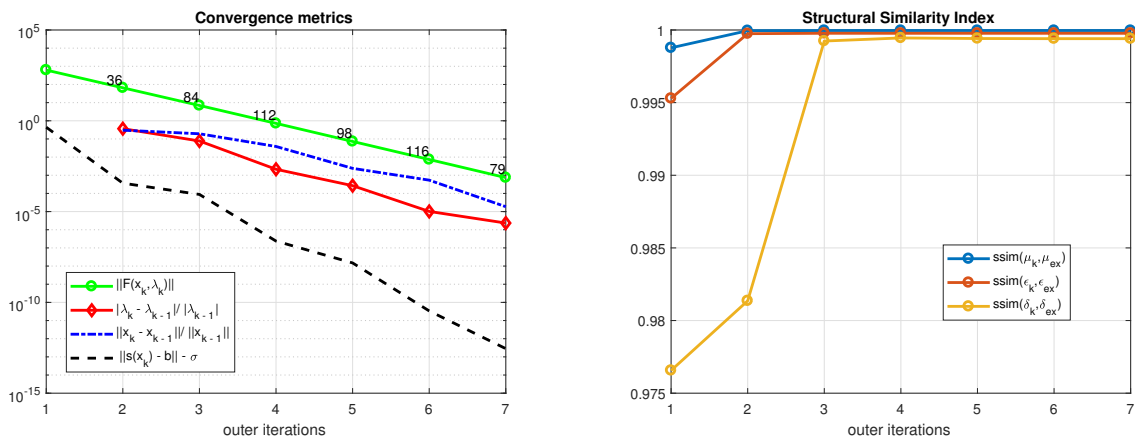


Figure 6: **Experiment 5.** (Left) Convergence metrics of a Talbot-Lau experiment with  $\text{npix} = 128$  and  $\text{nangles} = 5 \times \text{npix}$ . Tolerance is set to  $\tau = 10^{-6}$  and noiselevel 0.005. (Right) Structural Similarity index for the different components  $\mu_k$ ,  $\epsilon_k$  and  $\delta_k$  for the same experiment.

the true total regularization function (14).

The reconstructed solutions are shown in figure 5. In addition we also show the solution obtained by using standard form Tikhonov regularization, i.e. taking  $\Psi(x) = \|x\|^2$ , which is a very basic regularization technique that illustrates that the amount of noise in the data is non-trivial. We can clearly see that the reconstructed solutions are quite good and that the total variation regularization function nicely removes noise in the reconstruction, while still preserving edges in the images, especially compared to the solution obtained with standard form Tikhonov regularization. The  $\delta$  component in particular is very badly reconstructed when using Tikhonov regularization. This effect is less pronounced if we take a larger value  $v_0$  (close to one) since this implies that the noise in data is in a sense distributed more “equally” over the different components. If we take  $v_0$  very small, then  $\delta$  is reconstructed very badly even if we use total variation regularization, because this component becomes disproportionately affected by the noise in the data  $b$ . The same argument can be made about the  $\epsilon$  but in a less dramatic way. In general it holds that the component  $\mu$  is most easily reconstructed, which is not surprising if we inspect the forward model (13).

In figure 4 (left) we report some different convergence metrics for this experiment. We show convergence of the values  $\|F(x_k, \lambda_k)\|$  as always, as well as the relative difference of the iterates  $x_k$  and  $\lambda_k$ . In addition we also show the convergence of the constraint by plotting  $\|s(x_k) - b\| - \sigma$ . These first three metrics seem to converge in a similar fashion, while the latter value converges much more quickly. In the figure on the right, we show the Structural Similarity Index (SSIM) of the reconstructed solution compared with the exact solution. The closer this value is to 1 the more similar the two images are. It is interesting to see that this value stabilizes very quickly, even when

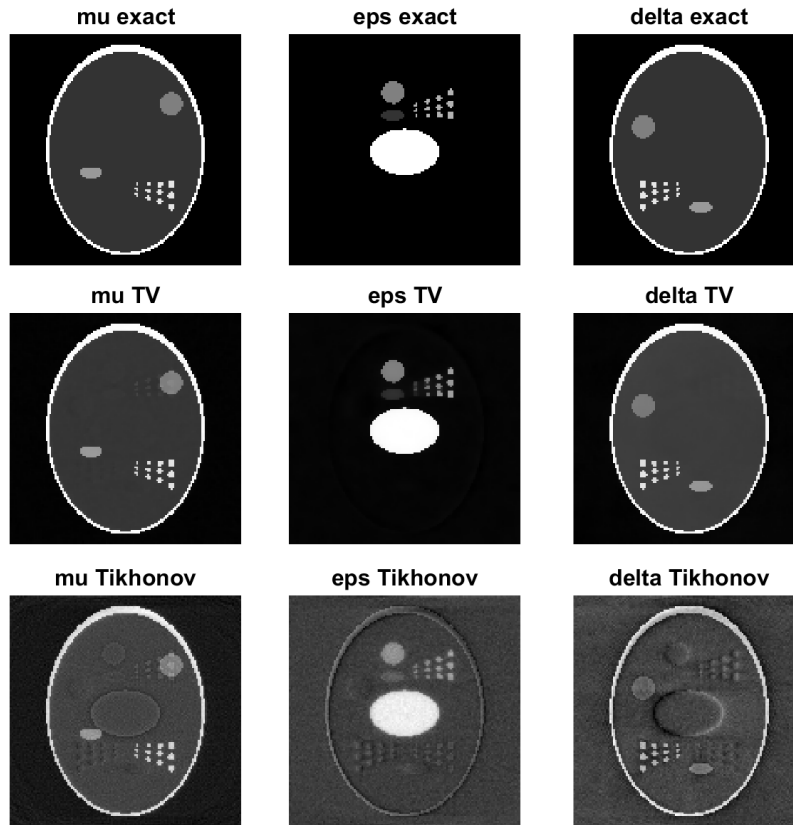


Figure 7: **Experiment 5.** The exact solution used in the experiment (top), the solution obtained by algorithm 2 with Total variation regularization (middle) and solution obtained using standard form Tikhonov regularization (bottom).

$\|F(x_k, \lambda_k)\|$  is not yet very small. Hence, it might be appropriate for practical problem to use a stopping criterion based on  $\|s(x_k) - b\| - \sigma$ , which decreases much more quickly. Similar observations were made by the authors in [7].

**Experiment 5.** For our final experiment we use entirely the same set-up as before, but now use a larger test-problem with `npix` = 128 as shown in figure 7 and with noiselevel 0.005. Furthermore, we now choose a moderate tolerance  $\tau = 10^{-3}$ . Results of this experiment can be found in figures 6 and 7. The same conclusions as in the previous experiment can be made here. A final interesting observation we make is that the reconstructions are merged together if we use standard form Tikhonov regularization to solve this problem, giving a very bad solution. This effect is much less pronounced when using total variation, where we only observe some of the ‘dots’ in the upper right corner of the  $\epsilon$  component in  $\mu$ .

## 5. Conclusions

In this work we have developed an efficient algorithm for the regularization of nonlinear inverse problems based on the discrepancy principle. By considering a linear approximation of the forward model using the Jacobian matrix, we obtain a quadratically constrained optimization problem which can be solved using the Projected Newton method. We prove that the solution of this equality constrained optimization problem results in a descent direction for a certain merit function, which can be used to formulate a formal line-search method for solving the inverse problem. We also formulate a slightly more heuristic version of the algorithm by loosening the tolerance of the solution of the sub-problems and removing the (seemingly unnecessary) line-search. We illustrate using the numerical experiments that these simplifications lead to a robust and computationally efficient method for solving the regularized nonlinear inverse problem. Moreover, we show that we can obtain very high quality reconstructions for Talbot-Lau x-ray phase contrast imaging using the newly proposed algorithm.

## Acknowledgments

This work was funded in part by the IOF-SBO project entitled ‘High performance iterative reconstruction methods for Talbot-Lau grating interferometry based phase contrast tomography’.

## References

- [1] Jorge Nocedal and Stephen Wright. *Numerical optimization*. Springer Science & Business Media, 2006.
- [2] Per Christian Hansen. *Discrete inverse problems: insight and algorithms*. SIAM, 2010.
- [3] Masao Fukushima, Zhi-Quan Luo, and Paul Tseng. A sequential quadratically constrained quadratic programming method for differentiable convex minimization. *SIAM Journal on Optimization*, 13(4):1098–1119, 2003.
- [4] Asen L Dontchev and R Tyrrell Rockafellar. *Implicit functions and solution mappings*, volume 543. Springer, 2009.
- [5] Patrick Fitzpatrick. *Advanced calculus*, volume 5. American Mathematical Soc., 2009.
- [6] Paul T Boggs and Jon W Tolle. A strategy for global convergence in a sequential quadratic programming algorithm. *SIAM journal on Numerical Analysis*, 26(3):600–623, 1989.
- [7] Jeffrey Cornelis and Wim Vanroose. Projected newton method for noise constrained  $\ell_p$  regularization. *Inverse Problems*, 36(12):125004, 2020.
- [8] Maximilian von Teuffenbach, Thomas Koehler, Andreas Fehring, Manuel Viermetz, Bernhard Brendel, Julia Herzen, Roland Proksa, Ernst J Rummeny, Franz Pfeiffer, and Peter B Noël. Grating-based phase-contrast and dark-field computed tomography: a single-shot method. *Scientific reports*, 7(1):1–8, 2017.
- [9] Wim Van Aarle, Willem Jan Palenstijn, Jan De Beenhouwer, Thomas Altantzis, Sara Bals, K Joost Batenburg, and Jan Sijbers. The astra toolbox: A platform for advanced algorithm development in electron tomography. *Ultramicroscopy*, 157:35–47, 2015.
- [10] Wim Van Aarle, Willem Jan Palenstijn, Jeroen Cant, Eline Janssens, Folkert Bleichrodt, Andrei Dabrovolski, Jan De Beenhouwer, K Joost Batenburg, and Jan Sijbers. Fast and flexible x-ray tomography using the astra toolbox. *Optics express*, 24(22):25129–25147, 2016.

**Appendix A. MATLAB code for generating Talbot-Lau test-problem**

The following MATLAB code is based on the ASTRA toolbox [9, 10].

```

1 function [A,D,phi0] = generate_testproblem(npix,nangles,nstep)
2 % Matlab function to generate Talbot-Lau test-problem.
3 % Input : - npix = number of pixels in each direction
4 %         - nangles = number of projection angles
5 %         - nstep = number of phase steps
6 %
7 % Output: - m x n matrix A, with m = npix*nangles and n = npix^2
8 %         - m x m finite difference matrix D
9 %         - m x 1 vector phi0: phase shift without the object
10 angles = linspace2(0,pi,nangles);
11 vol_geom = astra_create_vol_geom(npix,npix);
12 proj_geom = astra_create_proj_geom('parallel', 1.0, npix, angles);
13 proj_id = astra_create_projector('line', proj_geom, vol_geom);
14 matrix_id = astra_mex_projector('matrix', proj_id);
15 A = astra_mex_matrix('get', matrix_id);
16 astra_mex_projector('delete', proj_id);
17 astra_mex_matrix('delete', matrix_id);
18
19 D1 = spdiags([-ones(npix,1), +ones(npix,1)], [0 1], npix,npix);
20 I = speye(nangles); D = kron(I,D1);
21
22 phi_list = mod(0:(nangles - 1),nstep) + 1; %Index of the phase step
23 PHI_0 = linspace2(0,pi,nstep); PHIArray = zeros([npix nangles]);
24
25 for ii=1:npix, PHIArray(ii,:)= phi_list; end
26
27 PHIArray = PHIArray(:); phi0 = 0*PHIArray;
28
29 for ii=1:length(phi0), phi0(ii) = PHI_0(PHIArray(ii)); end
30
31 end

```